Journal of the Brazilian Society of Mechanical Sciences and Engineering (2019) 41:411
https://doi.org/10.1007/s40430-019-1915-4

REVIEW

Comparative study of different non-reflecting boundary conditions for compressible flows

Jhonatan Andrés Aguirre Manco[1] · **Marcio Teixeira de Mendonca**[1]

Received: 3 August 2018 / Accepted: 1 September 2019

Abstract
The numerical simulation of hydrodynamic stability and aeroacoustic problems requires the use of high-order, low-dispersion and low-dissipation numerical methods. It also requires appropriate boundary conditions to avoid reflections of outgoing waves at the boundaries of the computational domain. There are many different methods to avoid wave reflection at the boundaries such as the buffer zone and boundary conditions based on characteristic equations. This paper considers the use of a methodology called perfectly matched layer (PML). The PML is evaluated for the simulation of an acoustic pulse in a uniform flow and the Kelvin–Helmholtz instability in a mixing layer using the linear and nonlinear form of the Euler equation. PML results are compared with other non-reflecting boundary condition methods in terms of effectiveness and computational cost. The other non-reflecting boundary conditions implemented were the buffer zone (BZ), widely used in aeroacoustic and hydrodynamic problems, and the energy transfer and annihilation (ETA), a very simple boundary condition to be implemented. The results show that the PML is an effective boundary condition method, but can be computationally expensive. The PML is also more complex to implement and requires careful stability analysis. The other boundary conditions, the BZ and the ETA, are also effective and may perform better than the PML depending on the flow conditions. These two methods have an advantage in terms of robustness and are much simpler to implement than the PML.

Keywords PML · Non-reflecting boundary conditions · High-order numerical methods · Euler equations · Hydrodynamic stability

1 Introduction

In numerical simulations of transient phenomena such as aeroacoustics, laminar-turbulent transition and hydrodynamic stability, waves propagate in space and time. Therefore, it is important to implement boundary conditions that allow the outflow of these waves through the boundaries of the computational domain without affecting the solutions inside the domain. The correct treatment of the boundary conditions prevents numerical instabilities such that boundary disturbances do not interfere in the formation of eddy structures associated with instability or turbulence. It also reduces the simulation computational effort compared to solutions with far enough boundaries to avoid reflections from interfering with the flow structures in the region of interest.

The non-reflecting boundary conditions (NRBC) can be classified in three different types. The first one is based on the characteristic directions of the governing equations [8, 9, 11, 24]. It is based on the characteristic in one dimension and looses effectiveness when waves impinge on the boundary at an angle [5].

Another type of NRBC is based on the asymptotic solution of the governing equations in the far field. The governing equations are solved in the far field in a region where the flow is uniform or simpler. For the linearized Euler equations, Bayliss and Turkel [1] and Hagstrom, Haariharan and Thompson [10] derived outflow boundary conditions based on this approach. This type of boundary condition works quite accurately if the boundaries are placed sufficiently far, which results in a high computational cost. Another problem of the asymptotic boundary condition is that the asymptotic

Technical Editor: Jader Barbosa Jr., Ph.D.

✉ Jhonatan Andrés Aguirre Manco
jhonatanjaam@gmail.com

[1] Laboratório Associado de Combustão e propulsão, Instituto Nacional de Pesquisas Espaciais, Cachoeira Paulista, SP 12630-000, Brazil

Published online: 13 September 2019

solutions may not be always available for complex flows or nonlinear problems.

A third type of NRBC is based on damping zones, where the computational domain is extended and numerical filtering, stretching, damping or a combination of them is applied [6, 16, 25]. This type of boundary condition is frequently used because it is easy to implement and does not depend on the flow characteristics. The effectiveness of this method depends on the size of the damping zone and on the combination of the parameters that are used. However, in some problems, specially for high-order methods, quite large damping zones are used to get the desired precision, which means high computational cost.

The main objective of this work is the evaluation of three damping zone non-reflecting boundary conditions in a high-order numerical model for the solution of the linear and nonlinear Euler equations.

One of the damping zone methods of boundary condition treatment is the perfectly matched layer (PML). The PML is one of the most recent damping zone-type non-reflecting boundary condition developments, with promising results in effectiveness for damping outgoing waves and in terms of computational costs.

Hu [12] developed the PML for aeroacoustic and fluid mechanics applications based on Berenger [2] formulation for the solution of the Maxwell's equations. A latter work [13] demonstrated that Berenger's formulation could lead to numerical instabilities generated by the inconsistency between the waves phase velocity and the group velocity. To solve this problem, [13] proposed a stable formulation for the linearized Euler equations for uniform flows. Hu [14] extended Hu's work for the implementation of PML for non-uniform flows and linear Euler equations considering the case of the mixing layers. For non-uniform flows and non-linear Euler equations, [17] reformulated the PML.

In order to evaluate the PML, it will be compared to other two damping zone types of non-reflecting boundary conditions, the buffer zone and the energy transfer and annihilation (ETA). The buffer zone was formulated by Wasistho et al. [25] and is one of the most used in the literature. It is effective for absorbing Tollmien–Schlichting waves, presents good results in aeroacoustic as shown by Morris et al. [21] for supersonic jets, and was successfully applied on the solution of the Euler equations by Richards et al. [22].

The second non-reflecting boundary condition compared to the PML is the ETA. It was formulated by Edgar and Visbal [7] and used in aeroacoustic problems. The ETA is very simple to implement since it is based on grid stretching and filtering methods widely used in the simulation of hydrodynamic instability analysis and aeroacoustics problems.

The paper is organized as follows: first, the formulation of the PML, BZ and ETA is presented. Then, the numerical method used to solve the Euler equations is described. Finally, the results for the comparison of different types of non-reflecting boundary conditions are presented followed by conclusions.

2 Non-reflecting boundary conditions

The PML consists in defining a region around the domain of interest. In this region the governing equations being solved are modified to include dissipation terms which damp disturbance waves travel out of the domain of interest. Figure 1 shows schematically the domain of interest where solution of the Euler equations is sought and the boundary condition domain around it with dimensions D_x and D_y.

Hu [13, 14] proposed a well-posed and stable formulation for the PML which involves three steps; in the first step an appropriate space-time, $(\mathbf{x}, t)$, transformation is determined and applied to the governing equations.

$$\bar{t} = t + \beta \mathbf{x}, \tag{1}$$

where β is a coefficient that depends on the flow field. This transformation will ensure consistency between the group velocity and the phase velocity such that they are in the same direction [13].

As a second step, the equations are brought to the frequency domain using the Laplace transform and modified with a change of variables. The change of variables for a problem in two dimensions is defined as:

$$\frac{\partial}{\partial x} = \frac{1}{1 + i\sigma_x/\omega} \frac{\partial}{\partial \bar{x}}, \qquad \frac{\partial}{\partial y} = \frac{1}{1 + i\sigma_y/\omega} \frac{\partial}{\partial \bar{y}}, \tag{2}$$

where ω is the wave frequency and σ_x and σ_y are positive functions of the x, y coordinate directions and are known as the absorption coefficients.

In the final step, the non-reflecting boundary conditions are obtained rewriting the equations back in the spatial and temporal original coordinates.

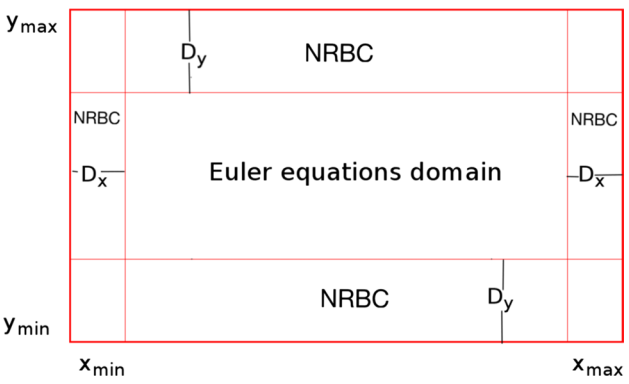

Fig. 1 Representation of the domain showing the region of interest and the boundary condition regions around it

2.1 PML formulation for the Euler equations

The PML and other non-reflecting boundary conditions were implemented for three different flow problems. The first implementation was for the linearized Euler equations for uniform flows. The second implementation was made to linearized Euler equations for non-uniform flows. Finally, the boundary conditions were implemented for nonlinear Euler equations to solve mixing layer-type flows.

For the linearized Euler equations for uniform flow, [13] proposed a stable PML, which ensures the elimination of perturbations in a damping zone. The equations are defined as:

$$\frac{\partial \mathbf{u}}{\partial t} + \mathbf{A}\frac{\partial \mathbf{u}}{\partial x} + \mathbf{B}\frac{\partial \mathbf{u}}{\partial y} + \sigma_y \mathbf{A}\frac{\partial \mathbf{q}}{\partial x} + \sigma_x \mathbf{B}\frac{\partial \mathbf{q}}{\partial y} + (\sigma_x + \sigma_y)\mathbf{u} + \sigma_x\sigma_y\mathbf{q} + \frac{\sigma_x M}{1-M^2}\mathbf{A}(\mathbf{u} + \sigma_y \mathbf{q}) = 0, \tag{3}$$

$$\frac{\partial \mathbf{q}}{\partial t} = \mathbf{u}, \tag{4}$$

$$\mathbf{u} = \begin{Bmatrix} \rho \\ u \\ v \\ p \end{Bmatrix}, \ \mathbf{A} = \begin{Bmatrix} u & \rho & 0 & 0 \\ 0 & u & 0 & \frac{1}{\rho} \\ 0 & 0 & u & 0 \\ 0 & \gamma p & 0 & u \end{Bmatrix}, \ \mathbf{B} = \begin{Bmatrix} v & 0 & \rho & 0 \\ 0 & v & 0 & 0 \\ 0 & 0 & v & \frac{1}{\rho} \\ 0 & 0 & \gamma p & v \end{Bmatrix}, \tag{5}$$

where $\mathbf{q}$ is an auxiliary variable, M is the free-stream Mach number and γ is the specific heat ratio. The solution vector components are the density (ρ), the velocity components in the streamwise (u) and normal (v) directions and the pressure (p).

The PML equation defined by Hu [14] for the linearized Euler equations for non-uniform flows is:

$$\frac{\partial \mathbf{u}}{\partial t} + \mathbf{A}\frac{\partial \mathbf{u}}{\partial x} + \mathbf{B}\left(\frac{\partial \mathbf{u}}{\partial y} + \sigma_x \frac{\partial \mathbf{q}}{\partial y}\right) + \mathbf{C}\left(\mathbf{u} + \sigma_x \mathbf{q}\right) + \sigma_x \mathbf{u} + \sigma_x \beta \mathbf{A}\mathbf{u} = 0, \tag{6}$$

with

$$\mathbf{C} = \begin{Bmatrix} 0 & 0 & \mathrm{d}\rho/\mathrm{d}y & 0 \\ 0 & u & \mathrm{d}u/\mathrm{d}y & 0 \\ 0 & 0 & 0 & 0 \\ 0 & 0 & 0 & 0 \end{Bmatrix} \quad \text{and} \quad \frac{\partial \mathbf{q}}{\partial t} = \mathbf{u}. \tag{7}$$

For the nonlinear Euler equations, [17] proposed the following formulation for the PML. The nonlinear Euler equations are first split in a mean flow $\overline{\mathbf{u}}$ independent of time and a time-dependent perturbation $\mathbf{u}'$. The vector $\mathbf{u}$ can be written as:

$$\mathbf{u} = \overline{\mathbf{u}} + \mathbf{u}'. \tag{8}$$

With this partition, it is more efficient to absorb only the temporal fluctuations.

Lin et al. [17] defined the PML for the nonlinear Euler equations for non-uniform flow as:

$$\frac{\partial \mathbf{u}}{\partial t} + \mathbf{A}\frac{\partial \mathbf{u}}{\partial x} + \mathbf{B}\frac{\partial \mathbf{u}}{\partial y} - \overline{\mathbf{A}}\frac{\partial \overline{\mathbf{u}}}{\partial x} - \overline{\mathbf{B}}\frac{\partial \overline{\mathbf{u}}}{\partial y} + \sigma_x \beta(\mathbf{u} - \overline{\mathbf{u}}) - \sigma_x \beta \mathbf{A}\mathbf{q_1} - \sigma_y \beta \mathbf{B}\mathbf{q_2} = 0, \tag{9}$$

with

$$\frac{\partial \mathbf{q_1}}{\partial t} + \sigma_x \mathbf{q_1} = \frac{\partial(\mathbf{u} - \overline{\mathbf{u}})}{\partial x} + \sigma_x \beta(\mathbf{u} - \overline{\mathbf{u}}), \tag{10}$$

$$\frac{\partial \mathbf{q_2}}{\partial t} + \sigma_y \mathbf{q_2} = \frac{\partial(\mathbf{u} - \overline{\mathbf{u}})}{\partial y}. \tag{11}$$

For the PML implementation, [14] recommended the following grid stretching in the PML zone:

$$\frac{\partial}{\partial n} \quad \rightarrow \quad \frac{1}{\alpha(n)}\frac{\partial}{\partial n}, \tag{12}$$

where n represents the coordinate direction x or y according to the direction of application of the PML and $\alpha(n)$ is a stretching function,

$$\alpha(n) = 1 + 2\left|\frac{n - n_0}{D}\right|^2. \tag{13}$$

The absorption coefficient σ used in the PML Eq. (3) as recommended by Hu [13] is:

$$\sigma_n = \sigma_{m(n)}\left|\frac{n - n_0}{D}\right|^{\beta}, \tag{14}$$

where $\sigma_{m(n)}$ controls the intensity of absorption within the PML. $\sigma_{m(x)}$ and $\sigma_{m(y)}$ were chosen according to [13].

2.2 Other non-reflecting boundary conditions

The first NRBC implemented for comparison with the PML is known as the buffer zone (BZ) and is based on numerical damping. As in the PML, to use this condition it is necessary to increase the domain including zones where the numerical damping will be applied (Fig. 1). Within the buffer zone, the amplitude of outgoing waves is damped to a value determined by a damping function σ. Defining $\overline{\mathbf{u}}^n = (\rho, u, v, p)$ as the solution vector at each time step, the buffer zone can be applied as:

$$\mathbf{u}^{n+1} = \overline{\mathbf{u}}^{n+1} - \sigma\left(\overline{\mathbf{u}}^{n+1} - \mathbf{u}_{\text{target}}\right). \tag{15}$$

where $\mathbf{u}^{n+1}$ is the solution vector for each time step after the application of the damping. The $\mathbf{u}_{\text{target}}$ used in (15) sets the required value $\overline{\mathbf{u}}$ on the buffer zone, which is defined depending on the problem. For the linearized Euler equations $\mathbf{u}_{\text{target}}$ is set to zero so that the perturbation that enters the buffer zone is removed from the base flow. For nonlinear Euler equations, $\mathbf{u}_{\text{target}}$ can be defined as the base flow for instantaneous variables as defined in (8). The damping function σ in (15) is defined in Sect. 4.

For the BZ the absorption coefficient, σ applied was based on Wasistho et al. [25]:

$$\sigma_n = (1 - C_1 n_b^2)\left(1 - \frac{1 - e^{C_2 n_b^2}}{1 - e^{C_2}}\right) \qquad \text{with,} \qquad n_b = \frac{n - n_s}{n_e - n_s}, \tag{16}$$

where n_s and n_e are points on the domain corresponding to the beginning and end of the damping zone, n represents the coordinates x and y, depending on the direction of application of the boundary condition. C_1 and C_2 define the transition mode of σ within the buffer zone and are set as $0 \leqq C_1 \leqq 0.1$ and $10 \leqq C_2 \leqq 20$. Several values of C_1 and C_2 were tested to find which presented the best results. The same grid stretching presented in (13) was used.

The third non-reflecting boundary condition implemented in this investigation is known as ETA (energy transfer and annihilation) and was formulated by Edgar and Visbal [7]. It is based on grid stretching and filtering. The energy of waves that goes out of the domain is transferred to higher-wavenumber waves using grid stretching. The set of high-wavenumber waves is eliminated by a high-order numerical filter. For the ETA non-reflecting boundary condition, the following grid stretching was applied:

$$n = dn\left(\frac{n - n_l}{dn}\right)^{\beta} + n_l, \tag{17}$$

where n_l is a domain point where the grid stretching begins, n represent the coordinates x or y and dn represents the grid spacing in the respective direction.

All non-reflecting boundary conditions were implemented on all boundaries, setting $D_x = D\Delta x$, $D_y = D\Delta y$ as the sizes of the non-reflecting boundary regions, D as the number of grid points and Δx and Δy de grid spacing.

3 Numerical method

Before the analysis of the different boundary condition techniques presented above, multiple spatial and temporal discretization methods were evaluated with respect to dispersion, dissipation and efficiency [19]. The objective was to determine the best discretization method to solve a mixing layer hydrodynamic stability problem.

The different methods were evaluated solving the wave equation in one dimension, as the wave equation is well posed and has analytic solution. In addition, it has characteristics similar to the mixing layer problem, in a sense that it is an unsteady, wave propagation problem, where the dispersion relation should be maintained.

For the discretization of the spatial and temporal terms, the following schemes were implemented:

Spatial Schemes

- Fourth-order central finite difference (DF4).
- Sixth-order compact finite difference (CPT) [18].
- Fourth-order dispersion relation-preserving finite difference (DRP) [23].

Temporal Schemes

- Fourth-order four-step Runge–Kutta (RK4).
- Fourth-order low-dissipation and low-dispersion Runge–Kutta (LDDRK4) [15].
- Fourth-order low-storage six-stage Runge–Kutta for nonlinear operators (RK46) [3].

In order to make a proper comparison, all schemes tested have the same order, except for the compact scheme, which achieves a high order with the same number of points of a fourth-order compact scheme by simply using different coefficients in its definition.

For the evaluation, a Gaussian pulse was transmitted and the best result was obtained with the compact (CPT) method with the Runge–Kutta six-step temporal scheme for nonlinear operators (RK46). Of all the schemes implemented, this scheme has the lowest dispersion and dissipation for the Gaussian pulse [19].

The compact scheme needs the solution of a tridiagonal matrix for each time step, which is more expensive computationally. The second best scheme is the DRP scheme, also with the six-step Runge–Kutta for nonlinear operators. This second explicit scheme is not as expensive as the compact finite difference scheme, but the results are similar. Therefore, the chosen scheme to discretize the Euler equations was the DRP for space discretization and the RK46 for time discretization.

In the numerical solution of the Euler equations, specially in the ETA non-reflecting boundary condition, a fourth-order 13-point numerical filter was used as proposed by Bogey and Bailly [4].

4 Results

This section presents the results for the numerical solution of the Euler equations with different types of boundary conditions. Section 4.1 presents results for the disturbance

pulse on a uniform flow and comparisons with exact analytic solutions, while Sect. 4.2 presents linear results for the spatial development of Kelvin–Helmholtz instability on a mixing layer. Section 4.2 also presents comparisons between numerical results and linear stability theory results as a verification test case. Finally, Sect. 4.3 presents results for the nonlinear development of Kelvin–Helmholtz instability on a mixing layer.

4.1 Linearized Euler equations, uniform flow

For the solution of the linearized Euler equations for a pressure pulse in a uniform flow with Mach number $M = 0.5$, the PML is compared to the BZ and ETA boundary conditions and with the analytic solution available for this simple case. A reference solution is also compared to the analytic solution. In the reference solution, the domain is sufficiently large to ensure that the initial pulse does not reach the boundaries during the total computation time and such that no reflections interfere with the solution. The reference domain size was defined as $(x_{\min}, x_{\max}) = (-400, 400)$ and $(y_{\min}, y_{\max}) = (-400, 400)$. The reference case was solved with the same numerical scheme presented in Sect. 3, and the numerical filter was applied every time step.

Table 1 summarizes the parameters used to implement the different non-reflecting boundary conditions in the numerical solution of the linearized Euler equations with uniform flow.

The Euler equations support three different waves: acoustic, entropy and vorticity waves. A presents the Gaussian pulses for the acoustic, vorticity and entropy waves used as initial conditions.

Figures 2, 3 and 4 show comparisons between the PML, BZ and ETA boundary conditions in terms of pressure contours for two different times, 30 and 50 time units. The lines of constant pressure go from − 0.15 to 0.15 in increments of .01. The PML and the ETA boundary condition initially will use 10 grid points on the damping zone, while the BZ will use 20 grid points. Twenty grid points is the minimum size supported by the BZ condition to avoid stability problems in the time interval evaluated. As will be shown, increasing the number of points in the NRBC zone for the ETA did not improve the results further. For the other NRBC, the

Table 1 Boundary condition parameters for the uniform flow test case

Domain	$x = (-50, 50)$, $y = (-50, 50)$
$(\Delta x, \Delta y, \Delta t)$	(1, 1, 0.5)
PML	$\sigma_{mx} = 2, \sigma_{my} = 2, \beta = 1, D = 10$
BZ	$C_1 = 0.01, C_2 = 20, D = 20$
ETA	$\beta = 2, D = 10$

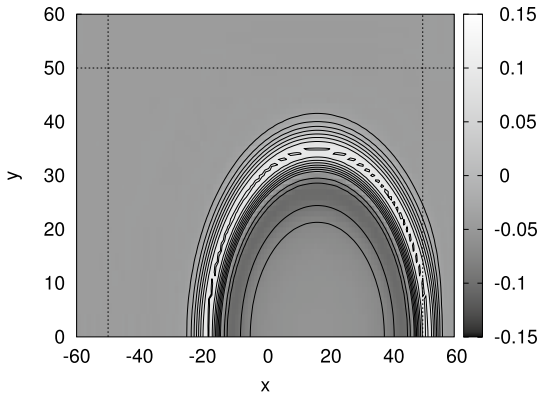

(a) PML, $t = 30$ time units

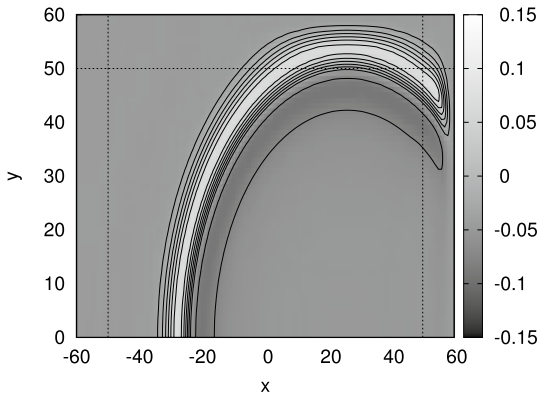

(b) PML, $t = 50$ time units

Fig. 2 Pressure contours for a pulse in a uniform flow with PML 10 boundary condition at two different times. Ten grid points on the NRBC zone

results improve increasing the number of grid points in the damping zone.

Qualitatively, the PML and the BZ give very similar results in the domain of interest. The ETA condition is not as accurate as the PML or the BZ and shows more reflections close to the boundaries during the passage of the wave front.

After the waves cross the outflow boundary zone, all three boundary conditions leave the domain of interest with little disturbance and resembles very well the analytic solution at 70 time units (Fig. 5). In the analytic solution it is not necessary to use damping zone, and the domain is $x = (-50, 50)$ and $y = (-50, 50)$.

To perform a quantitative comparison between the non-reflecting boundary conditions, the magnitude of the maximum reflection error in the pressure is measured. The pressure is measured across the section $x = 40$, 10 grid points inside the domain away from the right outflow boundary, for the three different boundary conditions implemented. The results are compared with pressure measured without using non-reflecting boundary condition and the pressure given by the analytic solution, available in this simple case.

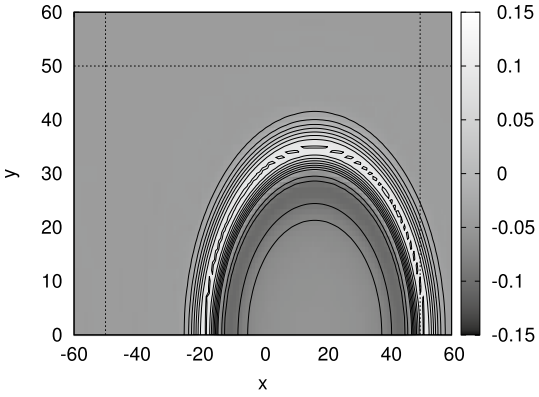

(a) BZ, $t = 30$ time units

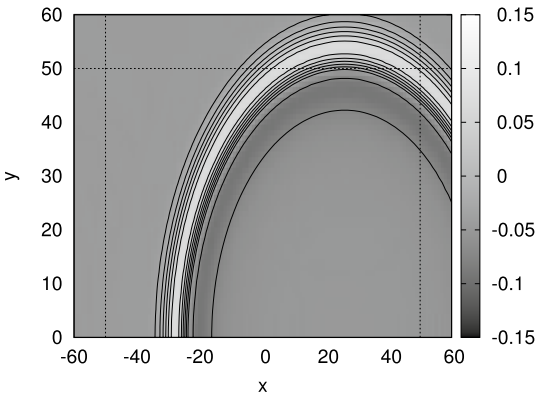

(b) BZ, $t = 50$ time units

Fig. 3 Pressure contours for a pulse in a uniform flow with buffer zone boundary condition at two different times. Twenty grid points on the NRBC zone

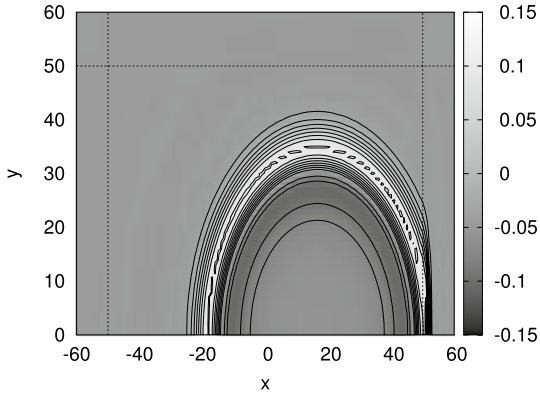

(a) ETA, $t = 30$ time units

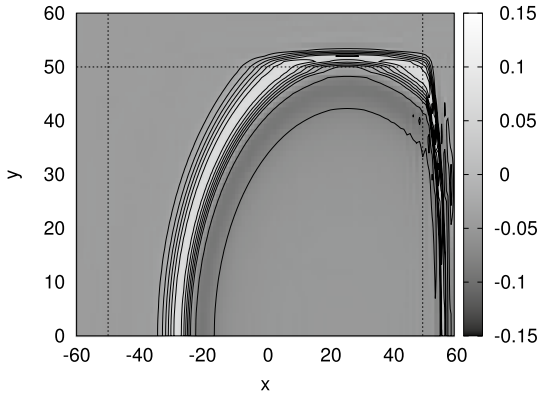

(b) ETA, $t = 50$ time units

Fig. 4 Pressure contours for a pulse in a uniform flow with ETA boundary condition at two different times. Ten grid points on the NRBC zone

The difference between the reference case and the analytic solution is also presented which allows the identification of errors associated with the numerical method without the influence of the boundary condition treatment.

In Fig. 6 a first comparison between the NRBCs implemented is presented. The numbers on the curve labels give the number of grid points in the damping region. The BZ condition used 20 grid points, because its behavior is unstable with fewer points. During the passage of the wave, the BZ gives the smallest pressure reflection. However, the number of grid point is greater. The worse performance of the ETA boundary condition is clear from the plot.

The improvement with increasing NRBC domain size is presented in Figs. 7, 8 and 9. The NRBC domain size was increased keeping dx and dy fixed and increasing the number of grid points from 10 to 20 and 30 grid points. For the PML and the BZ, increasing the NRBC domain size results in improved results. For the ETA, increasing the NRBC domain size beyond 20 grid points does not improve the results as seen in Fig. 8, where the curves for 20 and 30 grid points are on top of each other.

Figure 10 shows the final maximum pressure error using the best size of the absorption zone for the different boundary conditions. The best performance was obtained with the BZ, but the efficiency in terms of computational time has to be assessed. The corresponding computational cost of each NRBC will be evaluated next.

A comparison of computational time for the different non-reflecting boundary conditions with respect to the PML time is presented in Table 2. The values correspond to the CPU time required to run one hundred time steps. The only differences in computer codes are in the application of the different non-reflective conditions and on the fact that the filter for the ETA is applied at every Runge–Kutta step, while for the PML and BZ the filter is applied once at each time step. For the test cases considered, the PML and BZ conditions have similar performance in terms of computational time. The ETA has the smallest computational time and the worst results. The reason for using only 10 points for the ETA was that, as shown in Fig. 8, the results do not improve increasing the NRBC domain size, but the computational cost increases without additional benefits.

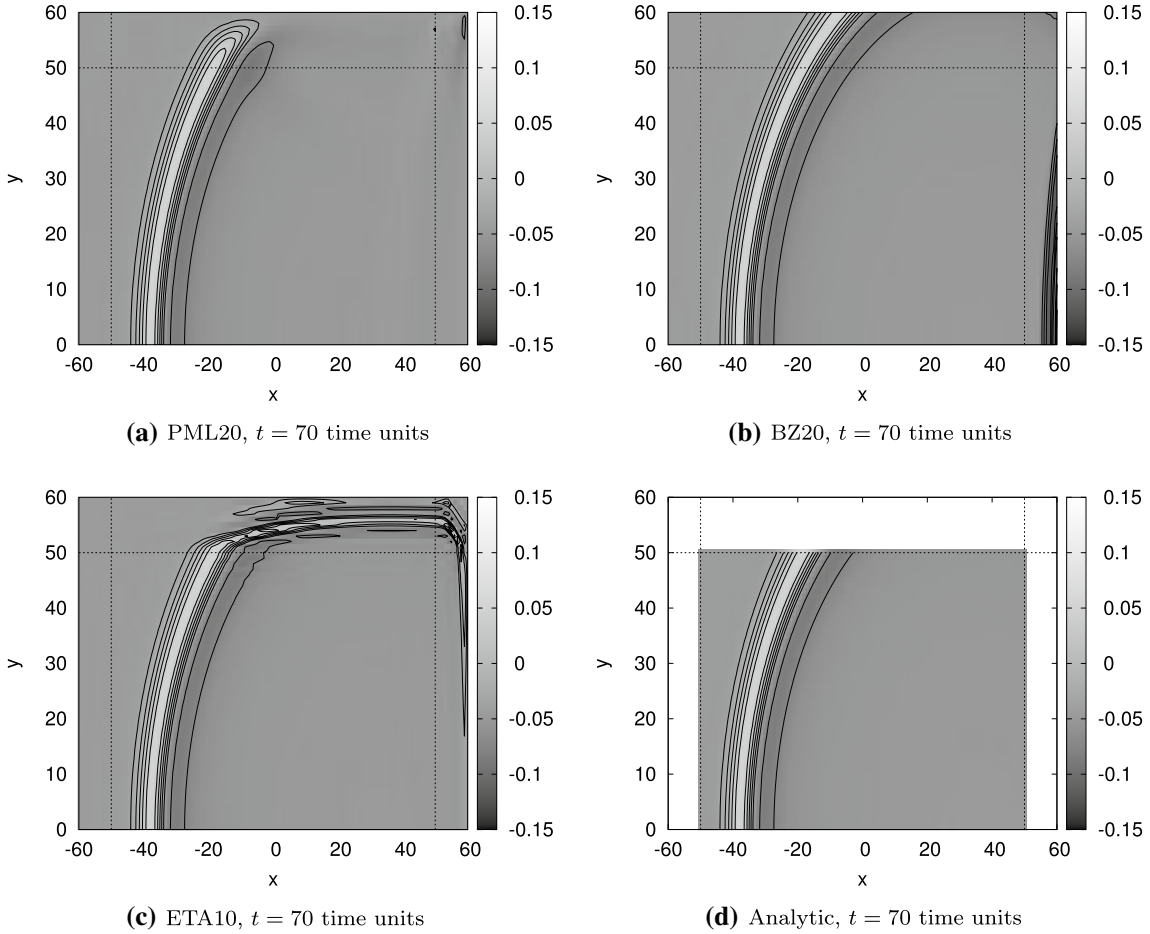

(a) PML20, $t = 70$ time units

(b) BZ20, $t = 70$ time units

(c) ETA10, $t = 70$ time units

(d) Analytic, $t = 70$ time units

Fig. 5 Pressure contours for a pulse in a uniform flow. Comparison between PML 20, BZ 20 and ETA 10 boundary conditions with the analytic solution at $t = 70$ time units

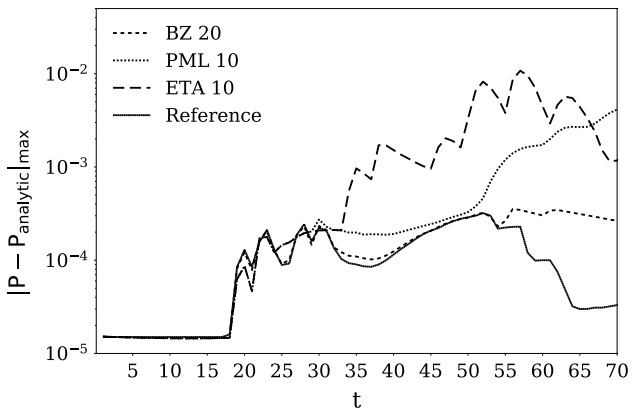

Fig. 6 Comparison of the maximum pressure error with respect to the analytic solution for different non-reflecting boundary conditions. Evolution in time at $x = 40$. The reference line refers to a solution without using NRBC, when the boundaries are sufficiently far to avoid reflections in the time interval evaluated

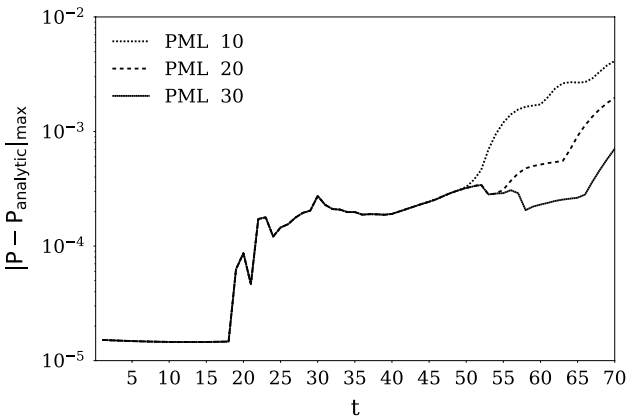

Fig. 7 Evolution in time of the maximum pressure error across $x = 40$ for different sizes of the PML non-reflecting boundary condition in relation to the analytic solution of a pressure pulse in a uniform flow

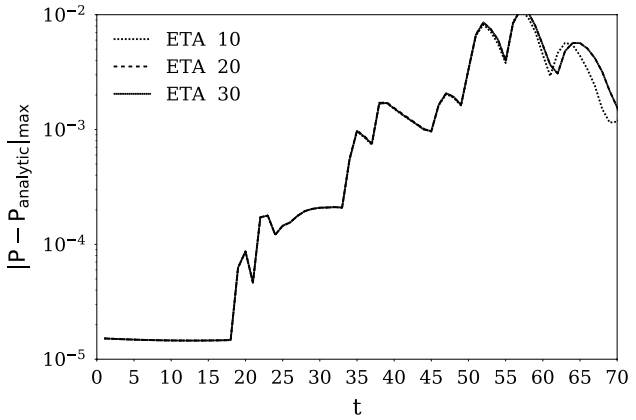

Fig. 8 Evolution in time of the maximum pressure error across $x = 40$ for different sizes of the ETA non-reflecting boundary condition in relation to the analytic solution of a pressure pulse in a uniform flow

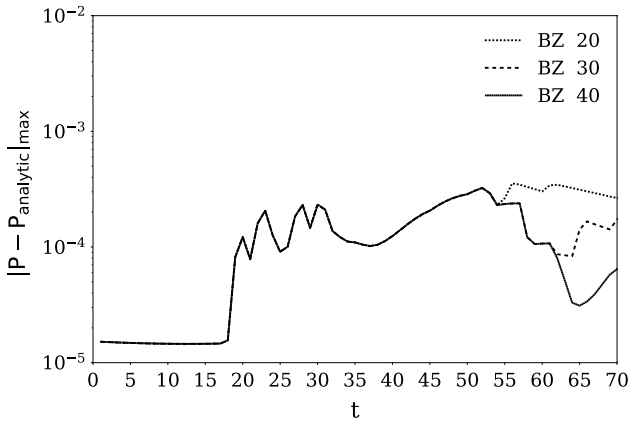

Fig. 9 Evolution in time of the maximum pressure error across $x = 40$ for different sizes of the BZ non-reflecting boundary condition in relation to the analytic solution of a pressure pulse in a uniform flow

Considering both the final maximum pressure error and the computational time for the propagation of a pressure pulse using the linear Euler equation, the best result is obtained with the BZ non-reflecting boundary condition.

4.2 Linearized Euler equations, non-uniform flow, mixing layer

This section presents comparisons between results obtained with the different types of NRBC defined previously considering the solution of the linearized Euler equations for a non-uniform flow. Before that, a validation test case is presented to verify the numerical model by comparing results with linear stability theory for the instability of compressible mixing layers.

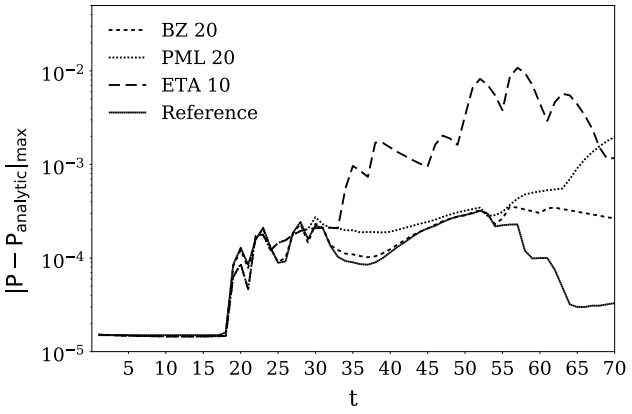

Fig. 10 Comparison of the maximum pressure error for each non-reflecting boundary condition in relation to the analytic solution for the propagation of a pressure pulse in a uniform flow. Evolution in time at $x = 40$. The reference line refers to a solution without using NRBC, where the boundaries are sufficiently far to avoid reflections in the time interval evaluated

Table 2 Computational time for each boundary condition type

Non-reflecting boundary condition	D (points)	Relative CPU time
PML	20	1.0
BZ	20	1.01
ETA	10	0.80

4.2.1 Verification test case

Before the presentation of comparisons between the different non-reflecting boundary conditions for a non-uniform flow, and to ensure that the numerical solution of the linearized Euler equations with the implemented non-reflecting boundary conditions is correct, a verification test case is presented considering only the PML.

Comparisons are presented with linear stability theory results for the growth rate of Kelvin–Helmholtz instability on a compressible mixing layer. The Mach number on the upper and lower streams is 0.8 and 0.2, respectively. The linear stability results were obtained by solving the compressible Rayleigh equation presented in C. For the Euler solver, the spatial amplification rate α_i is based on the kinetic energy growth along the streamwise direction. The comparison is presented in Fig. 11 for a range of frequencies ω, showing good agreement.

4.2.2 NRBC comparison for the non-uniform flow

Having verified the numerical model, this section presents comparisons between the different non-reflecting boundary

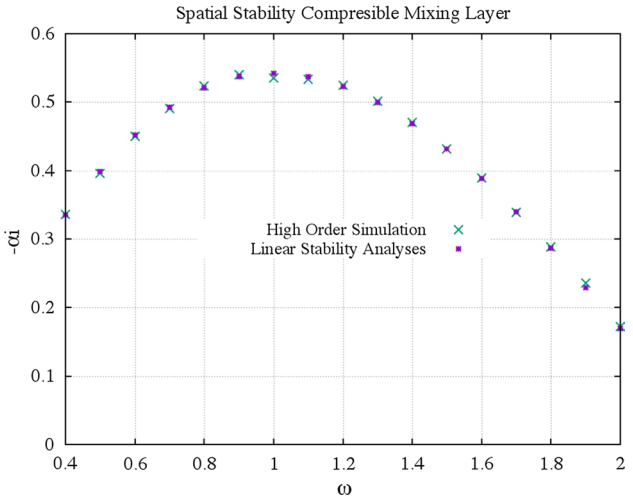

Fig. 11 Growth rate comparison between numerical solutions with PML boundary conditions and linear stability theory

conditions in a mixing layer flow. The initial conditions for a mixing layer flow solved with the linearized Euler equations are presented in B. To start the development of Kelvin–Helmholtz vortices, the mixing layer was perturbed with a Gaussian pressure pulse given by

$$s(x, y, t) = a \sin(wt) e^{-(ln2)[(x-x_0)^2+(y-y_0)^2]/r_0}, \quad (18)$$

where $a = 1$ defines the pulse amplitude, $w = \pi/2$ is the frequency, $x_0 = 0$ and $y_0 = 0$ define the pulse location and $r_0 = 0.05$ is the pulse thickness. The pressure pulse is applied at each time step of the Runge–Kutta during the complete simulation time.

The same three types of non-reflecting boundary conditions were implemented, BZ, PML and ETA. The size of the domain is $(x_{\min}, x_{\max}) = (-2, 8)$ and $(y_{\min}, y_{\max}) = (-2, 2)$. This domain is surrounded by the NRBC region. The time step is $dt = 0.01$, and the grid spacing is $dx = dy = 0.04$. The numerical filter was applied every time step in the PML and BZ case, but is applied at each Runge–Kutta stage for the ETA boundary condition.

As was done for the uniform flow cases, different absorption zone lengths were evaluated in order to find the best results with the smallest possible computational time. The size of the region where NRBC are applied depends on the number of grid points used. Table 3 gives the different parameters used for each different boundary condition type.

With the ETA, acceptable results were achieved with $D = 70$. The PML absorption zone was $D = 50$. The best result with the BZ was obtained using $D = 80$.

Figures 12, 13, 14 and 15 show the final pressure contours using the best size of the absorption zone for the different boundary condition types. The lines of constant pressure in the contours go from -0.15 to 0.15 in increments of .01. These figures allow the comparison between

Table 3 Boundary condition parameters for the linearized Euler equations and non-uniform flow

Domain	$x = (-2, 8)\, y = (-2, 2)$
$(\Delta x, \Delta y, \Delta t)$	(0.04, 0.04, 0.01)
PML	$\sigma_{mx} = 20, \sigma_{my} = 20, \beta = 1/1.416, D = 50$
BZ	$C_1 = 0.01, C_2 = 20, D = 80$
ETA	$\beta = 2, D = 70$

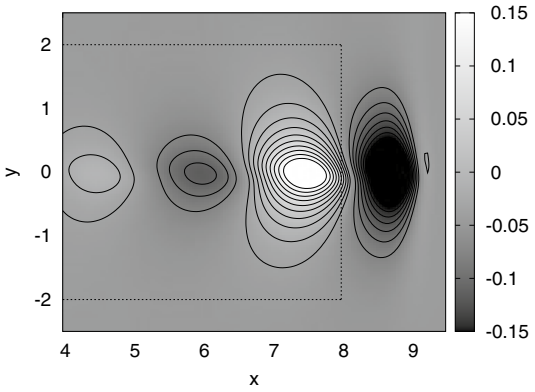

Fig. 12 Pressure contours after $t = 50$ time units using PML 50, fifty grid points on the damping zone. The dashed line represents the beginning of the damping region where the NRBC is applied

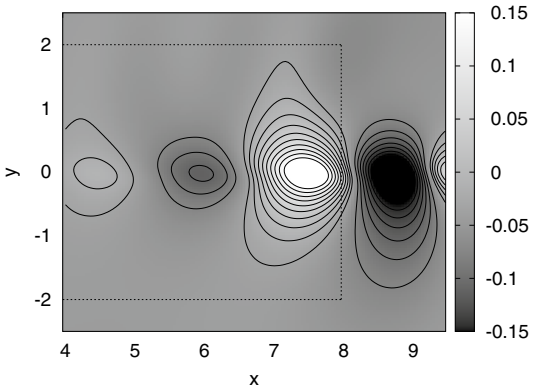

Fig. 13 Pressure contours after $t = 50$ time units using BZ 80, eighty grid points on the damping zone. The dashed line represents the beginning of the damping region where the NRBC is applied

the pressure contours using the different boundary conditions with respect to the reference case solution. The reference case, as in Sect. 4.1, uses a large domain such that the Kelvin–Helmholtz vortices do not reach the boundaries, avoiding reflections back into the domain of interest.

The pressure contours are similar, but the PML shows a better agreement with the reference case. The BZ is not as precise, but does not show the levels of reflection

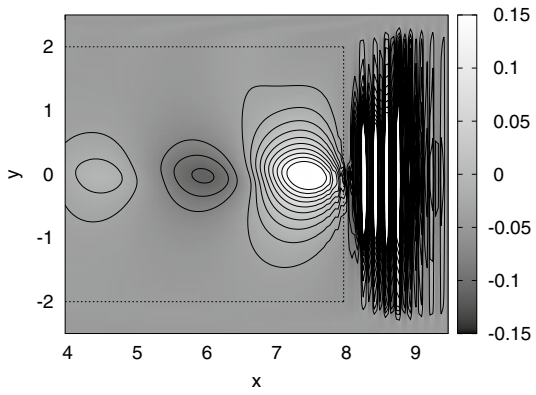

Fig. 14 Pressure contours after $t = 50$ time units using ETA 70, seventy grid points on the damping zone. The dashed line represents the beginning of the damping region where the NRBC is applied

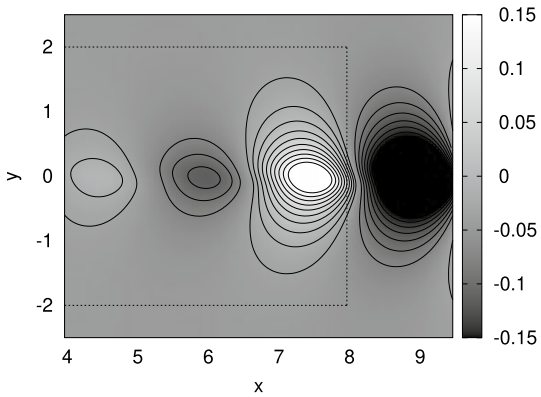

Fig. 15 Pressure contours after $t = 50$ time units without using NRBC. The boundaries are sufficiently distant to avoid reflections back into the domain of interest, marked with the dashed line

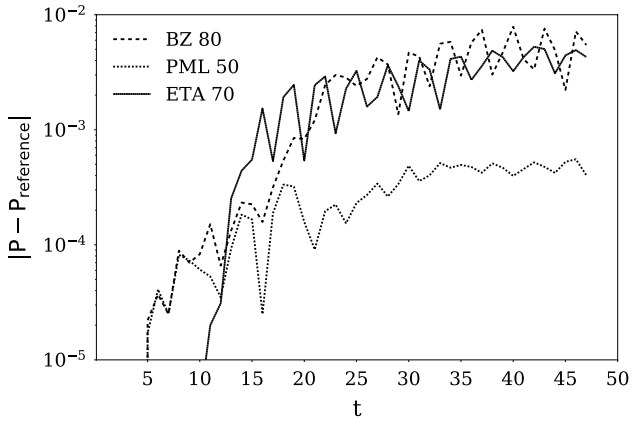

Fig. 16 Evolution in time of the maximum pressure error across $x = 7$ for the best size of the damping zone for the different non-reflecting boundary conditions in relation to the reference domain in the simulation of a mixing layer. The reference domain does not used NRBC, and the boundaries are sufficiently far to avoid reflections in the time interval evaluated

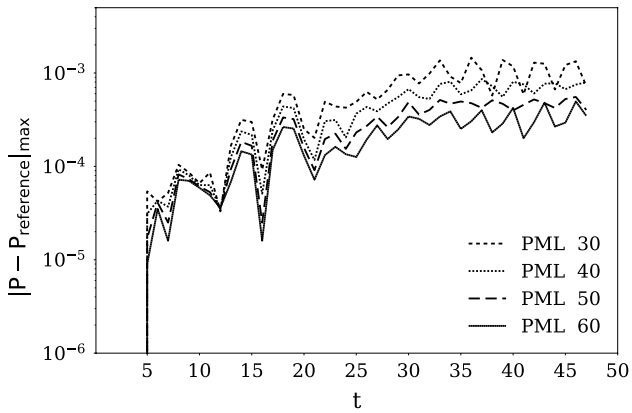

Fig. 17 Evolution in time of the maximum pressure error across $x = 7$ for different sizes of PML non-reflecting boundary condition in relation to the reference domain in the simulation of a mixing layer

presented by the ETA near the boundary of the NRBC zone on the right.

Similarly to the uniform flow case in Sect. 4.1, a quantitative comparison between the non-reflecting boundary conditions is presented. The comparison is based on the magnitude of the maximum reflection error in the pressure measured during the simulation time. The pressure is measured across the section $x = 7$, for the three different boundary conditions implemented, and the results are compared with the pressure measured without using non-reflecting boundary conditions, labeled the reference case. Figure 16 shows the best results selected in terms of the least reflection and lowest computational time. The numbers on the curve labels give the number of grid points in the NRBC region.

The improvement with increased NRBC domain size is presented in Figs. 17, 18 and 19. A relatively modest improvement is observed for the PML increasing the NRBC domain from 30 to 60. The same is true for the BZ increasing the NRBC from 60 to 80. For the ETA, increasing the NRBC domain size from 60 to 70, a significant improvement is observed, but beyond 70 grid points the results do not improve any further.

For the BZ and PML, considering the computational time, the sizes of $D = 80$ and $D = 50$, respectively, were selected. The PML solves additional equations on the NRBC zone, but requires fewer grid points to damp undesired reflections at the boundaries. The higher cost of solving additional equations is compensated by the use of fewer grid points.

Table 4 shows the computational time in seconds for each NRBC. The values correspond to the CPU time required to run one hundred time steps with respect to the PML time. The ETA is the fastest NRBC, but the results are worse than the PML results.

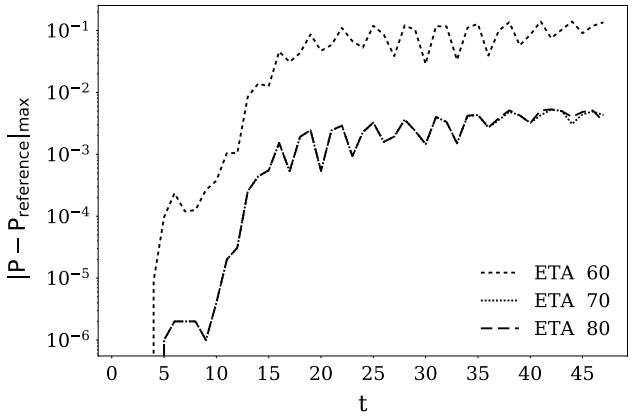

Fig. 18 Evolution in time of the maximum pressure error across $x = 7$ for different sizes of ETA non-reflecting boundary condition in relation to the reference domain in the simulation of a mixing layer. More points in this NRBC do not produce better results

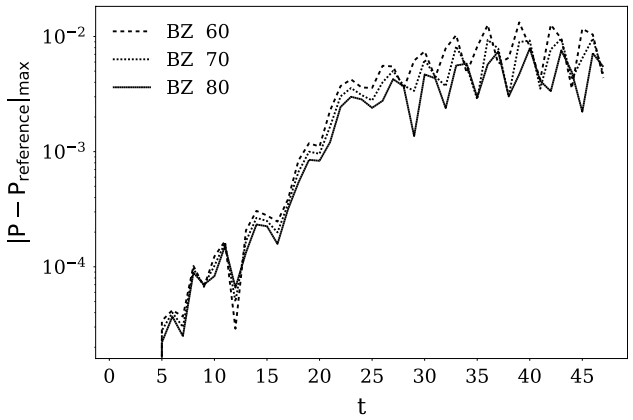

Fig. 19 Evolution in time of the maximum pressure error across $x = 7$ for different sizes of BZ non-reflecting boundary condition in relation to the reference domain in the simulation of a mixing layer

Table 4 Computational time for each boundary condition type

Non-reflecting boundary condition	D (points)	Relative CPU time
PML	50	1.0
ETA	70	0.92
BZ	80	1.11

Considering both the error in pressure and the CPU time, it is possible to conclude that the best boundary condition implemented in the linearized Euler equations for a mixing layer is the PML. The PML is more efficient computationally and has the lowest pressure difference in relation to the pressure in the reference case. The BZ and ETA present similar results in terms of percentage error with respect to the reference case, but the ETA has a lower computational time. It is worth emphasizing that the implementation of the BZ and ETA is simpler than the PML.

Table 5 Boundary condition parameters for the nonlinear Euler equations and non-uniform flow

Domain	$x = (-2,\ 10)\ y = (-1,\ 1)$
$(\Delta x,\ \Delta y,\ \Delta t)$	(0.05, 0.01, 0.01)
PML	$\sigma_{mx} = 40, \sigma_{my} = 40, \beta = 1/1.416, D = 60$
BZ	$C_1 = 0.01, C_2 = 20, D = 100$
ETA	$D = 50$

Table 6 Computational time for each boundary condition type

NRBC	D (points)	Relative CPU time
PML	60	1.0
ETA	50	0.57
BZ	100	1.07

4.3 Nonlinear Euler equations, non-uniform flow, mixing layer

Finally, the different non-reflecting boundary conditions, PML, ETA and BZ, were implemented for the numerical solution of nonlinear Euler equations for the mixing layer. For each type of non-reflecting boundary condition, different parameters were defined, using grid stretching with the respective absorption coefficients.

Table 5 shows the parameters that were used for the different boundary conditions for sizes of the absorption zones found to give the best results. For the ETA, the best results were achieved with $D = 50$, and the results do not improve significantly using higher sizes, following the same behavior as in the linear cases. For the BZ and the PML, the best results were achieved with $D = 100$ and $D = 60$, respectively. Above these NRBC domain sizes, the computational cost increases significantly in relation to the best results achieved with the ETA, $D = 60$.

Table 6 shows the computational times for the best results for each boundary condition. The values correspond to the CPU time required to run one hundred time steps relative to the PML CPU time.

Figures 20, 21, 22 and 23 show the final pressure contours using the best size of the absorption zone at $t = 50$ and the parameters defined in Table 5. The lines of constant pressure in the contours go from −0.6 to 0.8 in increments of 0.005. These figures allow the comparison between the pressure contours using the different boundary

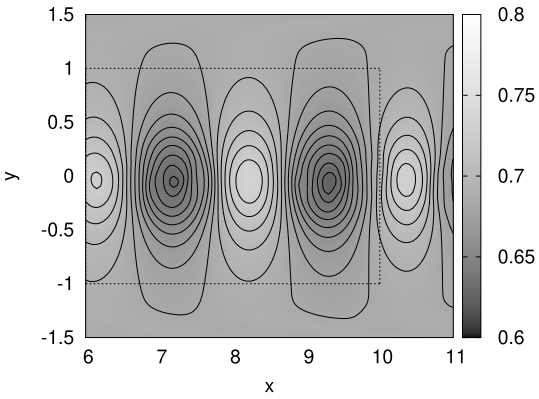

Fig. 20 Pressure contours after $t = 50$ time units using PML 60, sixty grid points on the NRBC zone. The dashed line represents the beginning of the damping region where the NRBC is applied

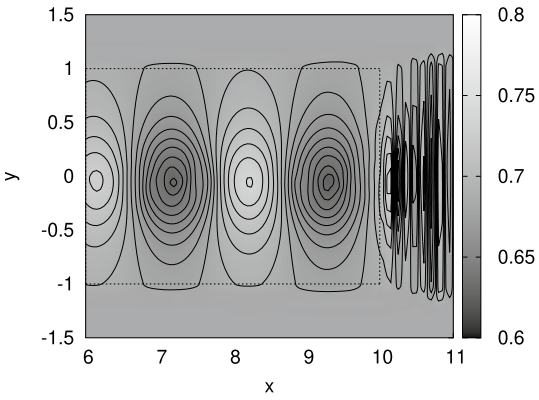

Fig. 21 Pressure contours after $t = 50$ time units using BZ 100, one hundred grid points on the NRBC zone. The dashed line represents the beginning of the damping region where the NRBC is applied

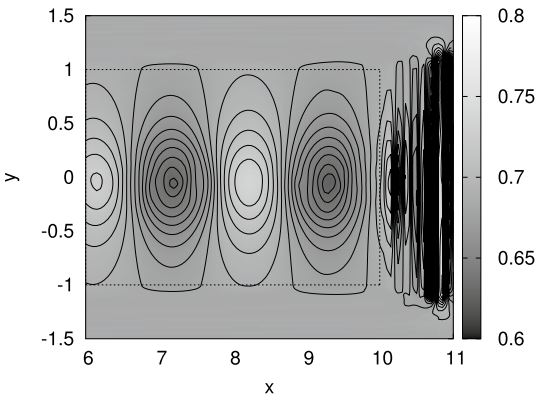

Fig. 22 Pressure contours after $t = 50$ time units using ETA 50, fifty grid points on the NRBC zone. The dashed line represents the beginning of the damping region where the NRBC is applied

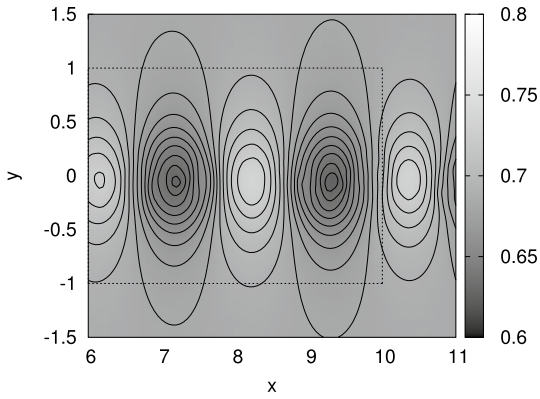

Fig. 23 Pressure contours after $t = 50$ time units without using NRBC. The boundaries are sufficiently far to avoid reflections back into the domain of interest, marked with the dashed line

conditions with respect to the reference case solution. The reference case, as in the previous section, uses a large domain such that the Kelvin–Helmhotz vortices do not reach the boundaries, avoiding reflections back into the domain of interest. The pressure contours for the different NRBC are very similar in the domain of interest, inside the dashed lines, and do not present significant differences.

As was done for the linear cases, a quantitative comparison between the non-reflecting boundary conditions is presented based on the magnitude of the maximum reflection error in the pressure measured during the simulation time. The pressure is measured across the section $x = 10$, for the three different boundary conditions implemented, and the results are compared with pressure measured without using non-reflecting boundary conditions, labeled the reference case. Figure 24 shows the best results selected in terms of the least reflection and lowest computational time. The numbers on the curve labels give the number of grid points in the NRBC region.

The improvement with increased NRBC domain size is presented in Figs. 25, 26 and 27. A relatively modest improvement is observed for the PML increasing the NRBC domain from 30 to 60. The same is true for the BZ increasing the NRBC size from 50 to 100. For the ETA, increasing the NRBC domain size from 50 to 60 does not improve the results any further.

Table 6 and Fig. 24 allow to conclude that the best boundary condition implemented in the nonlinear Euler equations for a mixing layer is the ETA. It is more efficient computationally and has the lowest pressure difference in relation to the pressure in the reference case. The BZ and PML present similar results in terms of both computational efficiency and percentage of error with respect to the reference case. It is worth emphasizing that the implementation of the BZ and ETA is simpler than the PML.

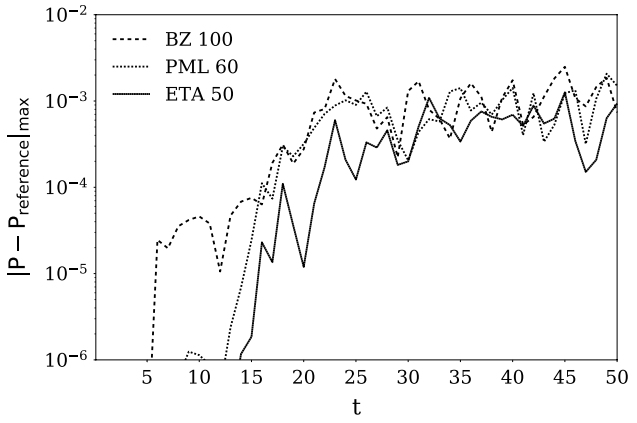

Fig. 24 Evolution in time of the maximum pressure error at $x = 10$ for the best damping zone size for the different non-reflecting boundary conditions with respect to the reference domain in the simulation of a mixing layer. The reference domain does not used NRBC, and the boundaries are sufficiently far to avoid reflections in the time interval evaluated

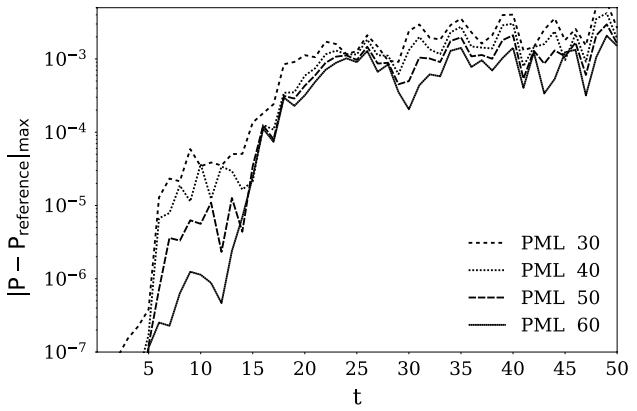

Fig. 25 Evolution in time of the maximum pressure error at $x = 10$ for different sizes of PML non-reflecting boundary condition in relation to the reference domain in the simulation of a mixing layer

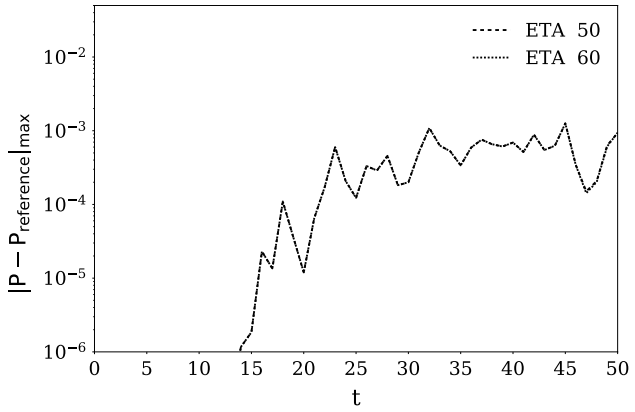

Fig. 26 Evolution in time of the maximum pressure error at $x = 10$ for different sizes of ETA non-reflecting boundary condition in relation to the reference domain in the simulation of a mixing layer

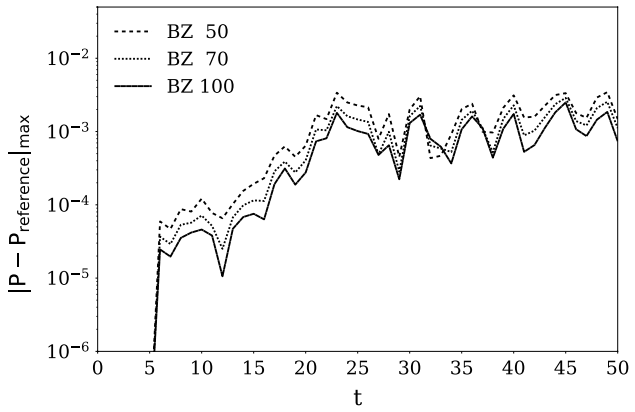

Fig. 27 Evolution in time of the maximum pressure error across $x = 10$ for different sizes of BZ non-reflecting boundary condition in relation to the reference domain in the simulation of a mixing layer

5 Conclusions

The present work presented comparisons between three different non-reflecting boundary condition methods, the PML, the BZ and the ETA. The comparisons allow an assessment of the PML NRBC method in terms of effectiveness and computational cost. Three different flow conditions were tested: the propagation of a pressure pulse in a uniform flow, the propagation of linear Kelvin–Helmhotz instabilities and the propagation of nonlinear Kelvin–Helmhotz instabilities. For the different cases evaluated, the good behavior of the three boundary conditions was evident. All three achieved satisfactory results when compared with a reference case.

For the uniform flow problem, the best NRBC is the BZ, which has a lower cost in terms of CPU time and the best performance in terms of disturbance absorption at the domain boundaries. The second best NRBC was the PML, in which increasing the damping zone size was able to mimic the BZ results, however, at a higher computation cost.

In the simulation of instabilities in a mixing layer, the PML performance was the best, being the maximum pressure error one order lower than the other two boundary condition methods.

In the most complex case evaluated, the nonlinear case for the propagation of instabilities in a mixing layer of the performance of all models was equivalent in terms of pressure error magnitude, but in terms of the computational cost the ETA needed one half of the time needed by the BZ and the PML to achieve the same level of accuracy.

Therefore, PML proved to be an efficient non-reflecting boundary condition, but with two disadvantages. First, the

PML can be computationally expensive when compared with the other two boundary conditions. In the cases where the PML was not the best boundary condition, the magnitude of the pressure error can be decreased using more points in the damping zone, which resulted in an increase in the computational cost. This increase in computational cost is due to the increased number of equations to be solved in the PML region. The second disadvantage is that the formulation of the PML is complex and can lead to numerical instabilities. Although PML transformations were defined by Hu to be implemented in the Euler and Navier–Stokes equations for different types of flows, it is necessary to study the PML stability for each new flow condition. Similar performance results can be achieved with simpler non-reflecting conditions such as the ETA and the BZ.

The boundary conditions BZ and ETA are effective in reducing reflections. They are simple to implement, and their formulation is independent of the equations solved. However, the BZ and ETA may have a lower performance when the damping zone size was not adequate.

Acknowledgements This work was financed by CAPES – Brazilian Higher Education Improvement Coordination within the Ministry of Education.

Appendix 1: initial conditions for uniform flow

For uniform flow, the following initial conditions were defined for acoustic, vorticity and entropy pulses:

$$\rho = A_0 \exp\left[-\ln(2)\left(\frac{(x+x_a)^2+(y+y_a)^2}{\delta_a}\right)\right] + C_0 \exp\left[-\ln(2)\left(\frac{(x+x_c)^2+(y+y_c)^2}{\delta_c}\right)\right], \tag{19}$$

$$u = B_0 y \exp\left[-\ln(2)\left(\frac{(x+x_b)^2+(y+y_b)^2}{\delta_b}\right)\right], \tag{20}$$

$$v = -B_0(x-x_b)\exp\left[-\ln(2)\left(\frac{(x+x_b)^2+(y+y_b)^2}{\delta_b}\right)\right], \tag{21}$$

$$P = -A_0(x-x_b)\exp\left[-\ln(2)\left(\frac{(x+x_b)^2+(y+y_b)^2}{\delta_b}\right)\right]. \tag{22}$$

The variables A_0, B_0 and C_0 are the amplitudes, and δ_a, δ_b and δ_c are the thicknesses for the acoustic, vorticity and entropy pulses, respectively. The positions x_a, x_b and x_c are the points of application of the different pulses. All pulses used in this work have unitary amplitude and a thickness of 16 and were located at the origin of the domain.

Appendix 2: initial conditions for a mixing layer

For the mixing layer, the initial conditions are:

$$\begin{Bmatrix}\rho_0\\ u_0\\ v_0\\ p_0\end{Bmatrix} = \begin{Bmatrix}\overline{\rho}(y)\\ \overline{M}_x(y)\\ 0\\ 1/\gamma\end{Bmatrix}, \tag{23}$$

where the streamwise non-dimensional velocity $\overline{M}_x$ distribution is

$$\overline{M}_x(y) = \frac{1}{2}\left[(M_{x1}+M_{x2}) + (M_{x1}-M_{x2})\tanh\left(\frac{2y}{\delta}\right)\right], \tag{24}$$

and the non-dimensional density is

$$\overline{\rho}(y) = \frac{1}{\overline{T}(y)}, \tag{25}$$

with the temperature distribution given by the Crocco–Busemann relation,

$$\overline{T}(y) = T_1\frac{\overline{M}_x - M_{x2}}{M_{x1}-M_{x2}} + T_2\frac{M_{x1}-\overline{M}_x}{M_{x1}-M_{x2}} + \frac{\gamma-1}{2}(M_{x1}-\overline{M}_x)(\overline{M}_x - M_{x2}). \tag{26}$$

The parameter δ is the thickness of the mixing layer, and $M_x(y)$ represents the streamwise velocity non-dimensionalized by the speed of sound. M_{x1} and M_{x2} are the non-dimensional velocities at the top and bottom of the mixing layer. Table 7 shows the parameters used in the mixing layer definition. A complete study of stability of this mixing layer is found in [20].

Appendix 3: basic disturbance equations

The compressible Rayleigh stability equation for pressure disturbance π in a two-dimensional, inviscid, parallel flow for a mixing layer can be written as:

$$\frac{\partial^2\pi}{\partial y^2} - \left(\frac{2}{M-c}\frac{\partial M}{\partial y} - \frac{\bar{T}'}{\bar{T}}\right)\frac{\partial\pi}{\partial y} - \alpha^2\left[1-\frac{1}{\bar{T}}(M-c)^2\right]\pi = 0. \tag{27}$$

Table 7 Parameters for the mixing layer definition

$M_{x1} = 0.8$	$M_{x2} = 0.2$
$T_1 = 1.0$	$T_2 = 0.8$
$\gamma = 1.4$	$\delta = 0.4$

To non-dimensionalize Eq. 27, reference values have been selected. $M = \bar{U}/a_0$ is the Mach number of the uniform flow, where $\bar{U}$ is the base flow velocity in the streamwise direction non-dimensionalized by a reference speed of sound a_0, $y = y'/l_0$ where y is the direction normal to the flow non-dimensionalized by a reference scale l_0, $T = T'/T_0$ where T is the base flow temperature non-dimensionalized by a reference temperature T_0, $\pi = p/(a_0^2\rho_0)$ where p is the pressure fluctuation, non-dimensionalized by $a_0^2\rho_0$, where ρ_0 is a reference density. $c = \omega/\alpha$ is the disturbance phase velocity, non-dimensionalized by the reference speed of sound a_0.

To solve Eq. 27 for spatial stability analyses, it is necessary to find the eigenvalues α for a particular ω for a nonlinear generalized eigenvalue problem:

$$\begin{aligned}\alpha^3\left(\frac{M^2}{\bar{T}}\bar{U}^3-\bar{U}\right)\pi\alpha^2\left(w-3\frac{M^2}{\bar{T}}\bar{U}^2w\right)\pi\\ +\alpha\left(3\frac{M^2}{\bar{T}}\bar{U}w^2-2\bar{U}'D+\bar{U}D^2+\frac{\bar{T}'}{\bar{T}}\bar{U}D\right)\pi\\ =\left(w^3\frac{M^2}{\bar{T}}+\frac{\bar{T}'}{\bar{T}}wD+wD^2\right)\pi,\end{aligned} \tag{28}$$

where D and D^2 represent the derivative operators $\partial/\partial y$ and $\partial^2/\partial y^2$, respectively.

To solve the nonlinear eigenvalue problem for α, the equations need to be linearized to a linear system of equations using the following transformation:

$$g = \alpha\pi, \tag{29}$$

$$\begin{aligned}\alpha^2\left(\frac{M^2}{\bar{T}}\bar{U}^3-\bar{U}\right)g+\alpha\left(w-3\frac{M^2}{\bar{T}}\bar{U}^2w\right)g\\ +\left(3\frac{M^2}{\bar{T}}\bar{U}w^2-2\bar{U}'D+\bar{U}D^2+\frac{\bar{T}'}{\bar{T}}\bar{U}D\right)g\\ =\left(w^3\frac{M^2}{\bar{T}}+\frac{\bar{T}'}{\bar{T}}wD+wD^2\right)p.\end{aligned} \tag{30}$$

Using:

$$z = \alpha g, \tag{31}$$

$$\begin{aligned}\alpha\left(\frac{M^2}{\bar{T}}\bar{U}^3-\bar{U}\right)z+\left(w-3\frac{M^2}{\bar{T}}\bar{U}^2w\right)z\\ +\left(3\frac{M^2}{\bar{T}}\bar{U}w^2-2\bar{U}'D+\bar{U}D^2+\frac{\bar{T}'}{\bar{T}}\bar{U}D\right)g\\ =\left(w^3\frac{M^2}{\bar{T}}+\frac{\bar{T}'}{\bar{T}}wD+wD^2\right)\pi,\end{aligned} \tag{32}$$

the final linear system of equations can be written as:

$$\begin{bmatrix}L_\pi & -L_g & -L_z\\ 0 & 1 & 0\\ 0 & 0 & 1\end{bmatrix}\begin{bmatrix}\pi\\ g\\ z\end{bmatrix}=\alpha\begin{bmatrix}0 & 0 & R_z\\ 1 & 0 & 0\\ 0 & 1 & 0\end{bmatrix}\begin{bmatrix}\pi\\ g\\ z\end{bmatrix}, \tag{33}$$

where

$$\begin{aligned}L_z &= w-3\frac{M^2}{\bar{T}}\bar{U}^2w,\\ L_g &= 3\frac{M^2}{\bar{T}}\bar{U}w^2-2\bar{U}'D+\bar{U}D^2+\frac{\bar{T}'}{\bar{T}}\bar{U}D,\\ L_\pi &= w^3\frac{M^2}{\bar{T}}+\frac{\bar{T}'}{\bar{T}}wD+wD^2,\\ R_z &= \frac{M^2}{\bar{T}}\bar{U}^3-\bar{U}.\end{aligned} \tag{34}$$

The eigenvalue problem 33 is solved using the spectral collocation method, with Chebyshev collocation points, using $N = 300$ points. As the collocations points are in the interval $[-1, 1]$, the mapping presented in (35) is used.

$$y = \beta\ \tan\left(\frac{\pi}{2N}\right). \tag{35}$$

where β controls the grid stretching and $\beta = 0.2$ was used.

References

1. Bayliss A, Turkel E (1982) Far field boundary conditions for compressible flows. J Comput Phys 48(2):182–199
2. Berenger JP (1994) A perfectly matched layer for the absorption of electromagnetic waves. J Comput Phys 114:195–200
3. Berland J, Bogey C, Bailly C (2006) Low-dissipation and low-dispersion fourth-order Runge–Kutta algorithm. Comput Fluids 35(10):1459–1463
4. Bogey C, Bailly C (2004) A family of low dispersive and low dissipative explicit schemes for flow and noise computations. J Comput Phys 194(1):194–214
5. Colonius T (2004) Modeling artificial boundary conditions for compressible flow. Annu Rev Fluid Mech 36:315–345
6. Colonius T, Lele SK, Moin P (1993) Boundary conditions for direct computation of aerodynamic sound generation. AIAA 31(9):1574–1582
7. Edgar NB, Visbal MR (2003) A general buffer zone-type nonreflecting boundary condition for computational aeroacoustics. In: AIAA paper 3300
8. Engquist B, Majda A (1977) Absorbing boundary conditions for numerical simulation of waves. Comput Phys 31:629–651
9. Giles MB (1990) Non reflecting boundary conditions for Euler equation calculations. AIAA 28:12
10. Hagstrom T, Haariharan SI, Thompson D (2003) High-order radiation boundary conditions for the convective wave equation in exterior domains. SIAM J Sci Comput 25(3):1088–1101. https://doi.org/10.1137/S1064827502419695

11. Hedstrom G (1979) Nonreflecting boundary conditions for nonlinear hyperbolic systems. J Comput Phys 30(2):222–237
12. Hu FQ (1996) On absorbing boundary conditions for linearized Euler equations by a perfectly matched layer. J Comput Phys 129(0244):201–219
13. Hu FQ (2001) A stable, perfectly mathed layer for linearized Euler equations in unsplit physical variables. J Comput Phys 173:455–480
14. Hu FQ (2005) A perfectly matched layer absorbing boundary condition for linearized Euler equations with a non-uniform mean flow. J Comput Phys 208:469–492
15. Hu FQ, Hussaini MY, Manthey JL (1996) Low-dissipation and low-dispersion Runge–Kutta schemes for computational acoustics. J Comput Phys 124(1):177–191
16. Israeli M, Orszag S (1981) Approximation of radiation boundary conditions. J Comput Phys 41:115–135
17. Lin KD, Li X, Hu F (2011) Absorbing boundary condition for nonlinear Euler equations in primitive variables based on the perfectly matched layer technique. Comput Fluids 40:333–337
18. Lele SK (1992) Compact finite difference schemes with spectral-like resolution. J Comput Phys 103(1):16–42
19. Manco JAA (2014) Non-reflecting boundary conditions for high order numerical simulation of compressible Kelvin–Helmholtz instability. Master's degree in Spatial Engineering and Technology, Instituto Nacional de Pesquisas Espaciais (INPE), São José dos Campos, INPE-17465-TDI/2256
20. Manco JAA, Freitas RB, Fernandes LM, Mendonca MT (2015) Stability of compressible mixing layers modified by wakes and jets. Procedia IUTAM 14:129–136
21. Morris PJ, Long LN, Scheidegger TE, Boluriaan S (2002) Simulations of supersonic jet noise. Int J Aeroacoust 1(1):17–41. https://doi.org/10.1260/1475472021502659
22. Richards S, Zhang X, Chen X, Nelson P (2004) The evaluation of non-reflecting boundary conditions for duct acoustic computation. J Sound Vib 270(3):539–557 (2002 I.M.A. Conference on Computational Aeroacoustics)
23. Tam CKW, Webb JC (1993) Dispersion-relation-preserving schemes for computational acoustics. J Comput Phys 107(184):262–281
24. Thompson KW (1990) Time-dependent boundary conditions for hyperbolic systems ii. J Comput Phys 89:439–461
25. Wasistho B, Geurts BJ, Kuerten JGM (1997) Simulation techniques for spacially evolving instabilities in compressible flow over a flat plate. Comput Fluids 26(7):713–739